Imaging Techniques

International Edition: DOI: 10.1002/anie.201604813
German Edition: DOI: 10.1002/ange.201604813

Assembly of a Highly Stable Luminescent Zn_5 Cluster and Application to Bio-Imaging

Ming-Hua Zeng, Zheng Yin, Ze-Hui Liu, Hai-Bing Xu, Ying-Chun Feng, Yue-Qiao Hu, Li-Xian Chang, Yue-Xing Zhang, Jin Huang,* and Mohamedally Kurmoo*

Abstract: *The assembly sequence of the coordination cluster $[Zn_5(H_2L^n)_6](NO_3)_4]\cdot 8H_2O\cdot 2CH_3OH$ (**Zn_5**, H_3L^n = (1,2-bis-(benzo[d]imidazol-2-yl)-ethenol) involves in situ dehydration of 1,2-bis(benzo[d]imidazol-2-yl)-1,2-ethanediol (H_4L) through the formation of the $[Zn(H_3L)_2]^+$ monomer, dimerization to $[Zn_2(H_3L)_2]^+$, dehydration of the ligand to $[Zn_2(H_2L^n)_2]^+$, and the final formation of the pentanuclear cluster. The cluster has the following special characteristics: 1) high stability in both refluxing 37% HCl and 27% NH_3, 2) low cytotoxicity, and 3) pH-sensitive fluorescence in the visible-to-near-infrared (Vis/NIR) region in the solid state and in solution. We have applied it as a fluorescent probe both in vivo and in vitro. Its H-bonding ability is the key to its affinity and selectivity for imaging lysosomes in HeLa cells and tumors in male BALB/C mice. It provides a new type of sensitive and biocompatible fluorescent probe for detecting small tumors (13.5 mm^3).*

There is currently major interest in the synthesis of coordination clusters as well as in their beautiful structures and rich functions.[1,2] While their solid-state properties are important, their solubility and stability in solution are as important for exploiting other functions, such as fluorescence in bioactivity and catalytic activity.[3] To advance the study of self-assembly by setting the foundation for the rational construction of coordination clusters with targeted connection, shape, and properties, a better understanding of their mechanism of formation involved is highly desired.[4] Though these mechanisms are quite complex, certain advances have been made, for example in polyoxometalates, coordination cages, and 3d-metal coordination clusters.[2,4,5] During the syntheses of clusters under hydro/solvothermal conditions, in situ ligand transformations are frequently observed.[6] The study of the cluster assembly process involving in situ ligand reactions is more difficult and has rarely been reported.[4,6]

Precise structural information of coordination clusters is mainly obtained by crystallography, while mass spectra (MS) can provide supplementary information about the cluster in solution.[2,4] The solid-state/solution structure information contributes to the identification of the existing molecular fragments of a cluster in solution and furthers the understanding of their diverse properties. For example, evaluating the stability and possible response behavior to changes in solution will help to explore new functions and application of coordination clusters. In our research, we have used a combination of crystallography and MS to unravel the mechanisms of the formation of a series of polynuclear 3d-metal clusters as well as the complexity of the clusters in solution.[2]

Previously, we observed the in situ dehydration of a 1,2-ethanediol-containing ligand (H_4L) to its 1,2-ethenol (H_3L^n) using a mixed H_2O/methanol solvothermal reaction, which induced the formation of a family of pentanuclear $[M_5(H_2L^n)_6]^{4+}$ (M = Co or Ni) clusters.[7] We therefore aimed to clarify the in situ ligand transformation and assembly mechanism of the **Zn_5** cluster because Zn has multiple isotopes, which can lead to better MS characterization. We also aimed to use Zn to replace the Au^I and Ru^{II}, which are commonly used as fluorescent probe for bio-imaging.[8] The advantages of Zn^{2+} are low-toxicity, high abundance in the body, and low cost. Several fluorescent Zn-based metal–organic frameworks or coordination clusters have been reported. However, the limited solubility and lower emission wavelengths restrict their usage as bioprobes.[9,10] As the planar $[H_2L^n]^-$ bridged the Zn^{2+} ions to form a quite rigid molecule with multiple inter-ligand interactions, we investigate its solid and solution optical properties in detail (Figure 1).

Interestingly, **Zn_5** exhibits unusually high stability as well as good affinity for HCl, NH_3, and neutral solvents. It has a broad fluorescence band centered at 540 nm and a narrow one at 650 nm. Exposure to acidic/basic conditions does not destroy the fluorescence of the cluster but does affect its intensity. This dependence on pH, along with several other

[*] Prof. Dr. M.-H. Zeng, Prof. Dr. H.-B. Xu, Y.-C. Feng, Y.-Q. Hu, L.-X. Chang, Dr. Y.-X. Zhang
Key Laboratory for the Chemistry and Molecular Engineering of Medicinal Resources, Guangxi Normal University
Guilin, 541004 (P.R. China)
and
College of Chemistry & Chemical Engineering, Hubei University
Wuhan, 430062 (P.R. China)
E-mail: zmh@mailbox.gxnu.edu.cn
Dr. Z. Yin
College of Chemistry and Chemical Engineering
Shaanxi University of Science & Technology
Xi'an 710021 (P.R. China)
Z.-H. Liu, Prof. Dr. J. Huang
Shanghai Key Laboratory of New Drug Design, School of Pharmacy
East China University of Science and Technology
Shanghai, 200237 (P.R. China)
E-mail: huangjin@ecust.edu.cn
Dr. M. Kurmoo
Institut de Chimie de Strasbourg, CNRS-UMR 7177
Université de Strasbourg
4 rue Blaise Pascal, 67070 Strasbourg (France)

Supporting information for this article (synthesis, measurement details, crystal data, TG, PXRD, mass spectra, optical spectra, TD-DFT calculations results, and bio-imaging photos) can be found under:
http://dx.doi.org/10.1002/anie.201604813.

 © 2016 Wiley-VCH Verlag GmbH & Co. KGaA, Weinheim

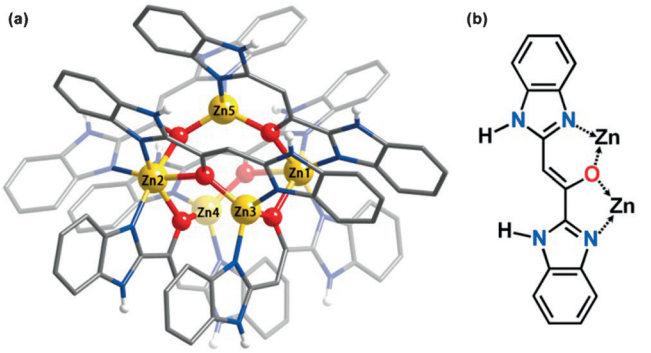

Figure 1. a) Illustration of the **Zn_5** cluster.[17] Zn = yellow, O = red, N = blue, and C = gray. b) The in situ generated H_2L^- ligand and its coordination to Zn.

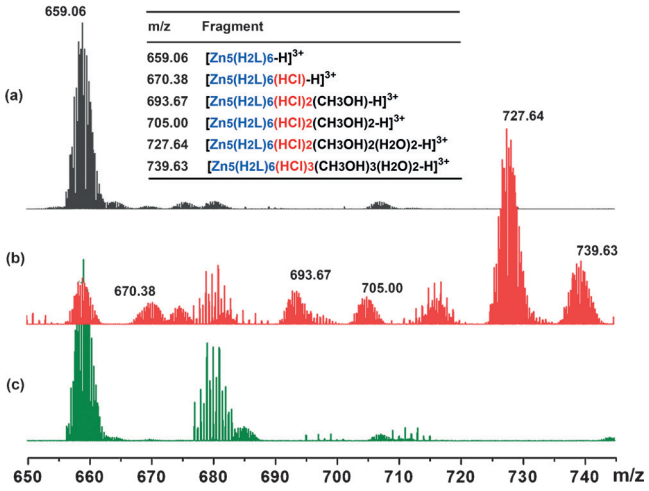

Figure 2. ESI-MS of methanol solutions of **Zn_5** as-synthesized (black), after refluxing in concentrated HCl (red) and aqueous NH_3 (green) for 24 h.

unexpected but desirable features, including low toxicity, biocompatibility, cellular permeability and probe retention, make **Zn_5** suitable for application as a pH-sensitive fluorescent probe for bio-imaging. Herein, we report its synthesis, structure, in situ ligand transformation and assembly mechanism by crystallography and MS, properties in both solid state and solution, and application in detecting cancerous tissue in vitro and in vivo.

The structure of **Zn_5** consists of three equatorial tetrahedra capped by two octahedra in a trigonal bipyramid shielded by the organic ligands. The special feature is that three pairs of parallel ligands bridge five Zn^{2+} ions through a μ_4-η_1,η_2,η_1 coordination to form a cluster with a diameter of circa 1.9 nm, in which there are six conjugated rings within each planar ligand. In addition, the rigid $[H_2L^n]^-$ is equipped with peripheral nitrogen atoms to coordinate with the Zn^{2+} ions and hydrogen atoms to form H-bonds. The clusters are charge balanced by NO_3^- and H-bonded to solvent molecules to give a close-packed solid-state structure. Several weak interactions were found within the cluster (Supporting Information, Tables S1–3 and Figures S1 and S2), which are likely responsible for the high chemical stability of the crystals (see below). The position, direction, and basicity of the peripheral N–H bonds of the benzimidazol are important features in its ability to form adducts with HCl and other solvents (see below).

To observe the in situ ligand dehydration and subsequent assembly of the **Zn_5** cluster, time dependent ESI-MS measurements of the reaction solution were performed. The MS of **Zn_5** was first investigated as a reference. All the peaks of **Zn_5** in methanol corresponded to the integral **Zn_5** cluster and its adducts with different solvent molecules, with up to 14 per cluster (Figure 2 and the Supporting Information, Table S4). Meanwhile, as **Zn_5** was very stable in most solvents during attempts to recover the transformed ligand by destroying it in concentrated HCl or aqueous NH_3, we further examined the treated samples by MS and powder x-ray diffraction (PXRD). Almost all the MS peaks of the acid- and base-treated samples were also associated with species containing the integral **Zn_5**, suggesting its high stability, which PXRD confirms in the crystalline state (Supporting Information, Figures S3–5). A surprising finding is that several observed peaks correspond to prominent adducts of the **Zn_5** core with HCl and NH_3. Such extremely high stability and great affinity for acid, base and neutral molecules are unique and rarely observed in coordination clusters.[2]

To study the assembly process of **Zn_5**, the reactants were first stirred at room temperature for 1 h ($t = 0$) followed by heating at 140 °C in Teflon-lined steel bombs. Aliquots of the solutions were sampled after 30, 90, 150, and 210 min, and 6, 12, and 24 h. A white powder precipitate was observed within 90 min. As time elapses, yellow crystals of **Zn_5** are apparent to the naked eye and become larger and more abundant while the white powder gradually disappears. The MS at $t = 0$ and 30 min (Supporting Information, Figures S6 and S7) are dominated by $[Zn(H_3L)_2{+}H]^+$ (m/z 651.15) and $[Zn_2(H_3L)_2{-}H]^+$ (m/z 715.05), suggesting that monomer and dimer precursors were initially formed. Once the heating time exceeds 150 min, two peaks appear at m/z 989.94 and 679.03 and their intensities consistently increase at the expense of that of the monomer. The former corresponds to $[Zn_5(H_2L^n)_6{-}2H]^{2+}$, a characteristic signal of **Zn_5**. The latter is identified as $[Zn_2(H_2L^n)_2{-}H]^+$, which is the dehydrated form of $[Zn_2(H_3L)_2{-}H]^+$. Though these two dimers were not isolated from the solution, structures with similar ligands are known in the literature, which are usually segments in which a pair tetrahedral Zn^{2+} ions are bridged by two ligands.[11] It also should be noted that, except for $[Zn_2(H_2L^n)_2{-}H]^+$ and $[Zn_5(H_2L^n)_6{-}2H]^{2+}$, no other peaks correspond to fragments containing the dehydrated H_3L^n ligand (expected at m/z 277.1). Based on these findings, the in situ ligand dehydration and **Zn_5** assembly are proposed to follow a process in which the $[Zn(H_3L)_2 + H]^+$ monomer is first formed, then dimerized to $[Zn_2(H_3L)_2{-}H]^+$, followed by dehydration of the ligand to $[Zn_2(H_2L^n)_2{-}H]^+$, and finally the formation of the $[Zn_5(H_2L^n)_6{-}2H]^{2+}$ cluster. The coordination of the Zn^{2+} ions to hydroxy groups activated the α-H and β-OH groups, inducing the in situ dehydration. For comparison, solvothermal treatment of H_4L did not generate dehydrated H_3L^n, confirming the crucial role of the ligand

 © 2016 Wiley-VCH Verlag GmbH & Co. KGaA, Weinheim

coordination with metal ions (Supporting Information, Figure S8).

During the monitoring of the reaction process, bright fluorescence was observed with the naked eye when the reaction solution containing **Zn_5** was placed under a UV-lamp (Supporting Information, Figure S9). Therefore, we performed a detailed analysis of the optical properties of **Zn_5**. A DMSO solution of **Zn_5** displays two intense absorption bands at 353 and 375 nm with a shoulder at 410 nm (Supporting Information, Figure S10). The spacing between the two strong peaks is of the order of one vibrational mode of the ligand but the energy difference between 410/375 nm is higher. We associated the high energy pair with the $\pi\rightarrow\pi^*$ transition.[12] The shoulder peak is assigned to the $^1\pi\rightarrow\pi$ transition of the ligand, which is supported by time-dependent density functional theory calculations (Supporting Information, Figure S11 and Table S5).

The room temperature fluorescence of **Zn_5** in DMSO solution displays a strong broad band at 540 nm together with a sharp shoulder at 650 nm under excitation at $\lambda_{ex}=430$ nm (Figure 3 and the Supporting Information, Figures S12–16).

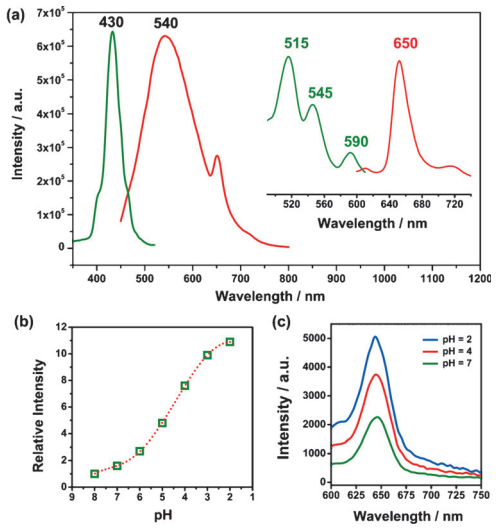

Figure 3. a) Emission (red, $\lambda_{ex}=430$ nm) and excitation profile (green, $\lambda_{em}=540$ nm) of **Zn_5** in DMSO solution. Inset: expanded emission (red, $\lambda_{ex}=515$ nm) and excitation profile (green, $\lambda_{em}=650$ nm) of the Vis/NIR region. The pH-dependent emission intensity of **Zn_5** (1 μg mL^{-1}) in PBS solution with b) $\lambda_{ex}=410$ nm and c) $\lambda_{ex}=530$ nm.

Further analysis shows that the 650 nm emission can be generated by excitation at a wide range of visible wavelengths, with multiple resonance peaks at 515, 545 and 590 nm. The presence of 650 nm peaks in the spectra of the isostructural **Co_5** and **Ni_5** confirms that the emission originates from the organic ligands (Supporting Information, Figures S17 and S18). The lifetimes, circa 1–2 nanoseconds for all the luminescent bands of the **M_5** (M = Zn, Co, Ni) family (Supporting Information, Table S6), confirmed they are not from a triplet state.[12] Thus, the emission band at 540 nm is ascribed to the intraligand $\pi\rightarrow\pi^*$ transition. While the emission at 650 nm is assigned to the interligand transition within the cluster, which results from the intermolecular π–π stacking interaction with a distance of circa 3.3 Å. Such multiple excitation and emission bands are rarely observed in coordination clusters. They originate from the special ligand configuration that results from the penta-nuclear core, including planarity, rigidity, six conjugated rings, and parallel ligands with short distances.[9] The observed emission, which is close to the Vis/NIR region, is also uncommon for Zn coordination clusters, as most of them have emission bands located in the UV/Vis region, originating from intra-ligand transitions.[9]

As **Zn_5** shows affinity to HCl and NH_3, we investigated whether pH affects the fluorescence of **Zn_5**, especially the emission at 650 nm. The pK_a of **Zn_5** was determined to be 4.8 using a Sirius T3 apparatus at 25 °C in aqueous solution (Supporting Information, Figure S19). The PBS buffer solutions of **Zn_5** with pH ranging from 2 to 8 exhibit similar absorption spectra with almost unchanged intensity (Supporting Information, Figure S20). However, the fluorescence of **Zn_5** is sensitive to the solution pH. When the pH decreased from 7 to 2, an 8-fold and 2.5-fold enhancement is observed for the emission peaks at 500 nm and 650 nm, respectively, in a PBS solution (Figure 3 and the Supporting Information, Figure S21). Thus, **Zn_5** exhibits different pH sensitivity at different emission wavelengths. The pH dependence may stem from the reversible protonation and de-protonation of the uncoordinated imidazole nitrogen, which leads to alterations of the π electronic charge densities of the ligands (Figure 1).[13]

The high chemical stability, emission in the Vis/NIR range, pH sensitivity, and a pKa located in the tumor pH range, are characteristics of **Zn_5** that meet the requirements for pH-sensitive fluorescent bioprobes.[10] To clarify whether a similar a fluorescence response occurs in biological organisms, we investigated the application of **Zn_5** in cultured cells. **Zn_5** is photostable in both BSA and mouse serum (Supporting Information, Figures S22 and S23). Additionally, **Zn_5** has negligible cytotoxicity for HeLa (human cervical carcinoma cells), 293T (transformed human kidney cell line) and CHO-K1 (Chinese hamster ovary cell) (Supporting Information, Figure S24). **Zn_5** was then used to target lysosomes in living cells because of their acidic microenvironment. Co-localization experiments involving **Zn_5** were performed in HeLa cells using LysoTracker Red (LTR) as a known lysosome-specific fluorescent probe. The distribution of the fluorescence from **Zn_5**, shown in blue, co-localized and overlapped well with the red fluorescence from LTR, indicating **Zn_5** can selectively display lysosomes in living cells because of the acidic microenvironment (Supporting Information, Figure S25). The fluorescence response of **Zn_5** to pH changes in HeLa cells was also tested under the control of bafilomycin A1, which is a selective inhibitor for lysosomal acidification. With increased concentration of bafilomycin A1, lysosomal pH increased and the blue fluorescence of **Zn_5** within the cells gradually decreased, whereas the red fluorescence of LTR remained essentially unchanged (Supporting Information, Figure S26), confirming the feasibility of using **Zn_5** to monitor pH changes in living cells.

Several reports have indicated that the tumor extracellular microenvironment is more acidic than normal tissues,

 © 2016 Wiley-VCH Verlag GmbH & Co. KGaA, Weinheim

which is an important characteristic for differentiating tumors.[14] Encouraged by the success in imaging lysosomes and monitoring pH changes of the microenvironment in live cells, we explored the use of $\mathbf{Zn_5}$ in tumor imaging. The in vivo tumor imaging was investigated in A375 tumor-bearing mice and was performed by an IVIS Spectrum CT imaging system with excitation at 450–485 nm and emission at 630–650 nm using appropriate filter sets. Although excitation in the visible light region, which has low tissue penetration, can limit in vivo imaging, both the 2D and 3D images still show that the tumor is distinguishable from other tissues with good fluorescence contrast (Figure 4 and the Supporting Information, Figures S27–30). The fluorescence intensity gradually disappeared 6 h post-injection, suggesting that the probe can be metabolized by the body. Although the fluorescence signal becomes weaker when the A375 tumor size is decreased, it is still distinguishable for tumors as small as circa 13.5 mm^3. Therefore, $\mathbf{Zn_5}$ is a new fluorescent tumor indicator, which can effectively detect tumors in mice in vivo, owing to the acidic tumor microenvironment. There are only a few pH-sensitive NIR fluorescent probes that can distinguish tumors. Most reported examples are organic dyes[15] and nanoparticles.[16] Owing to its multiple fluorescence bands and pH response in solution, $\mathbf{Zn_5}$ can be used for bio-imaging in complex biological systems.

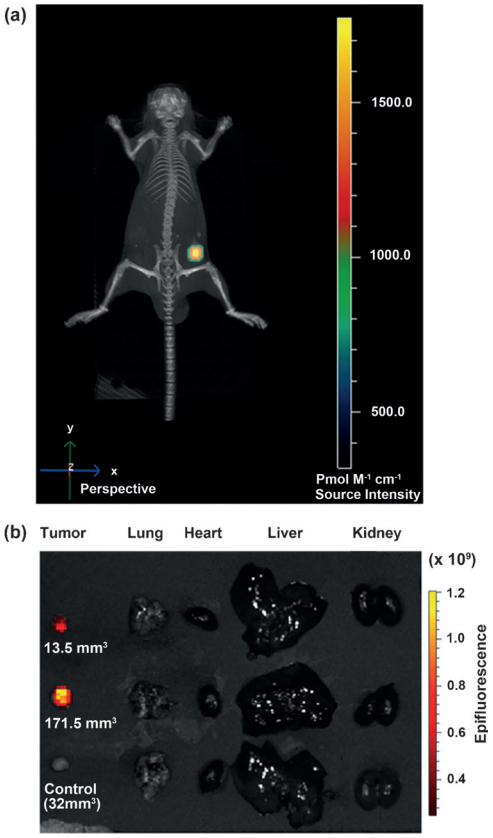

Figure 4. a) 3D fluorescence imaging of the mice bearing A375 tumor after intravenous injection of $\mathbf{Zn_5}$. b) Fluorescence imaging of tumors of different sizes and vital organs collected from the experimental mice bearing A375 tumor after intravenous injection of $\mathbf{Zn_5}$.

In conclusion, we have shown the sequence of both the in situ ligand dehydration and assembly of a polynuclear cluster through a solvothermal reaction by crystallography and MS. The solid-state and solution structural information explained the numerous unusual properties of the $\mathbf{Zn_5}$ cluster including its high stability, affinity for various molecules, multiple fluorescence bands, and pH sensitivity. These positive characteristics were applied in bio-imaging, in which $\mathbf{Zn_5}$ functioned as a pH-responsive Vis/NIR fluorescent bioprobe with negligible toxicity. The distinct fluorescence at tumor sites provides new opportunities for non-invasive in vivo imaging of tumors as small as 13.5 mm^3. To the best of our knowledge, the present $\mathbf{Zn_5}$ is the first example of a pH-sensitive Vis/NIR probe from a 3d-metal cluster. This work presented a vivid example of the relevance of solid and solution structures in guiding the functional exploration of a coordination cluster. This first report of tumor imaging using a small Zn cluster also suggests the potential to develop inexpensive, 3d-metal coordination molecules from biologically abundant metals for bio-imaging and disease diagnosis in the future.

Acknowledgements

This work was supported by the National Science Foundation of China for Distinguished Young Scholars (No. 21525101), the NSFC (No. 91422302, 21371037, and 21571165), the NSFGX (No. 2014GXNSFFA118003, CMEMR2014-A02), BAGUI scholar program (2014A001) and the Project of Talents Highland of Guangxi province. M.K. thanks the CNRS-France.

Keywords: 3d-metal coordination cluster · bio-imaging · fluorescence probes · pH sensitivity · Zn clusters

How to cite: *Angew. Chem. Int. Ed.* **2016**, *55*, 11407–11411
Angew. Chem. **2016**, *128*, 11579–11583

[1] a) F. Xu, H. Miras, R. Scullion, D.-L. Long, J. Thiel, L. Cronin, *Proc. Natl. Acad. Sci. USA* **2012**, *109*, 11609–11612; b) X.-J. Kong, L.-S. Long, Z.-P. Zheng, R.-B. Huang, L.-S. Zheng, *Acc. Chem. Res.* **2010**, *43*, 201–209.
[2] a) M.-H. Zeng, M.-X. Yao, H. Liang, W.-X. Zhang, X.-M. Chen, *Angew. Chem. Int. Ed.* **2007**, *46*, 1832–1835; *Angew. Chem.* **2007**, *119*, 1864–1867; b) Y. Q. Hu, M. H. Zeng, K. Zhang, S. Hu, F. F. Zhou, M. Kurmoo, *J. Am. Chem. Soc.* **2013**, *135*, 7901–7908; c) Q. Chen, M.-H. Zeng, L.-Q. Wei, M. Kurmoo, *Chem. Mater.* **2010**, *22*, 2114–2119; d) K. Zhang, M. Kurmoo, L.-Q. Wei, M.-H. Zeng, *Sci. Rep.* **2013**, *3*, 3516.
[3] Y.-M. Yang, Q. Zhao, W. Feng, F.-Y. Li, *Chem. Rev.* **2013**, *113*, 192–270.
[4] H. N. Miras, E. F. Wilson, L. Cronin, *Chem. Commun.* **2009**, 1297–1311.
[5] a) C.-H. Zhan, R. S. Winter, Q. Zheng, J. Yan, J. M. Cameron, D.-L. Long, L. Cronin, *Angew. Chem. Int. Ed.* **2015**, *54*, 14308–14312; *Angew. Chem.* **2015**, *127*, 14516–14520; b) Q. F. Sun, S. Sato, M. Fujita, *Nat. Chem.* **2012**, *4*, 330–333.
[6] X.-M. Chen, M.-L. Tong, *Acc. Chem. Res.* **2007**, *40*, 162–170.

 © 2016 Wiley-VCH Verlag GmbH & Co. KGaA, Weinheim

[7] Y.-L. Zhou, F.-Y. Meng, J. Zhang, M.-H. Zeng, H. Liang, *Cryst. Growth Des.* **2009**, *9*, 1402 – 1410.
[8] a) D. L. Ma, H. Z. He, K. H. Leung, D. S. H. Chan, C. H. Leung, *Angew. Chem. Int. Ed.* **2013**, *52*, 7666 – 7682; *Angew. Chem.* **2013**, *125*, 7820 – 7837; b) X. K. Wan, W. W. Xu, S. F. Yuan, Y. Gao, X. C. Zeng, Q. M. Wang, *Angew. Chem. Int. Ed.* **2015**, *54*, 9683 – 9686; *Angew. Chem.* **2015**, *127*, 9819 – 9822.
[9] a) E. E. Langdon-Jones, S. J. A. Pope, *Chem. Commun.* **2014**, *50*, 10343 – 10354; b) Y. J. Cui, Y. F. Yue, G. D. Qian, B. L. Chen, *Chem. Rev.* **2012**, *112*, 1126 – 1162; c) S. L. Zheng, X. M. Chen, *Aust. J. Chem.* **2004**, *57*, 703 – 712.
[10] a) Z. Guo, S. Park, J. Yoon, I. Shin, *Chem. Soc. Rev.* **2014**, *43*, 16 – 29; b) J. Y. Han, K. Burgess, *Chem. Rev.* **2010**, *110*, 2709 – 2728.
[11] G. Mund, A. J. Gabert, R. J. Batchelor, J. F. Britten, D. B. Leznoff, *Chem. Commun.* **2002**, 2990 – 2991.
[12] a) J. Heine, K. Muller-Buschbaum, *Chem. Soc. Rev.* **2013**, *42*, 9232 – 9242; b) H.-B. Xu, L.-Y. Zhang, J. Ni, H.-Y. Chao, Z.-N. Chen, *Inorg. Chem.* **2008**, *47*, 10744 – 10752.
[13] H. J. Kim, C. H. Heo, H. M. Kim, *J. Am. Chem. Soc.* **2013**, *135*, 17969 – 17977.
[14] a) S. K. Parks, J. Chiche, J. Pouyssegur, *Nat. Rev. Cancer* **2013**, *13*, 611 – 623; b) Y. Urano, D. Asanuma, Y. Hama, Y. Koyama, T. Barrett, M. Kamiya, T. Nagano, T. Watanabe, A. Hasegawa, P. L. Choyke, H. Kobayashi, *Nat. Med.* **2009**, *15*, 104 – 109.
[15] a) Q. Yuan, Y. Wu, J. Wang, D.-Q. Lu, Z.-L. Zhao, T. Liu, X.-B. Zhang, W.-H. Tan, *Angew. Chem. Int. Ed.* **2013**, *52*, 13965 – 13969; *Angew. Chem.* **2013**, *125*, 14215 – 14219; b) A. Wallabregue, D. Moreau, P. Sherin, P. M. Lorente, Z. Jarolimova, E. Bakker, E. Vauthey, J. Gruenberg, J. Lacour, *J. Am. Chem. Soc.* **2016**, *138*, 1752 – 1755.
[16] C. He, K. Lu, W. Lin, *J. Am. Chem. Soc.* **2014**, *136*, 12253 – 12256.
[17] CCDC 1470928 contains the supplementary crystallographic data for this paper. These data are provided free of charge by The Cambridge Crystallographic Data Centre.

Received: May 17, 2016
Revised: July 16, 2016
Published online: August 16, 2016

 © 2016 Wiley-VCH Verlag GmbH & Co. KGaA, Weinheim